Digital Signal Processing 87 (2019) 104–111

Contents lists available at ScienceDirect

Digital Signal Processing

www.elsevier.com/locate/dsp

Bounded non-linear covariance based ESPRIT method for noncircular signals in presence of impulsive noise

Jiacheng Zhang [a], Tianshuang Qiu [a,*], Shengyang Luan [b], Houjie Li [c]

[a] Faculty of Electronic Information and Electrical Engineering, Dalian University of Technology, Dalian 116024, China
[b] School of Electrical Engineering and Automation, Jiangsu Normal University, Xuzhou 221116, China
[c] College of Information and Communication Engineering, Dalian Minzu University, Dalian, Liaoning, 116600, China

ARTICLE INFO

Article history:
Available online 28 January 2019

Keywords:
Bounded non-linear covariance
DOA
ESPRIT
Noncircular signal

ABSTRACT

Among the most important approaches in the study of DOA estimation, ESPRIT-like methods have received considerable attentions and have been widely applied in practical applications. Although many of the latest approaches have considered various performance requirements, the robustness to impulsive noise warrants further investigation. Inspired by the idea of bounded non-linear covariance (BNC), a novel subspace based method for DOA estimation is proposed in this paper. Named NC-BNC-ESPRIT, this method uses the BNC matrix to create a signal subspace of extended array outputs and it can handle the DOA estimation for noncircular (NC) signals in presence of impulsive noise. Simulation experiments and theoretical analysis are provided to verify this methods' superiority over existing approaches and proof of its robustness is provided in the appendix.

1. Introduction

In the recent decades, direction of arrival (DOA) estimation for source localization has received intensive attentions and this technique has been applied to many wireless communications systems, including radar, sonar and so on [1]. Many recent contributions have been made in the field of subspace based methods and multiple signal classification (MUSIC) [2] is one of the most famous ones. By applying eigenvalue decomposition to the covariance matrix of received array outputs, MUSIC obtains DOAs through the relationship between the signal subspace and noise subspace. For example, using the roots of a polynomial formed from the noise subspace, Root-MUSIC [3,4] improves the DOA estimation performance. Employing the time-reversal (TR) techniques, TR-MUSIC [5–7] achieves a higher resolution. Although MUSIC based methods exhibit outstanding performances, their requirements in computation and storage are considerable. In addition to MUSIC, the estimating signal parameter via rotational invariance technique (ESPRIT) [8], plays an equally important role in subspace based DOA estimation methods. It was proposed to reduce the computational complexity and it can achieve a high resolution through the invariance structure of a sensor array. Due to its superior performance, many ESPRIT-like approaches have been made as well. By considering the multi-invariance (MI) structure of array outputs, MI-ESPRIT [9] further improves the DOA estimation accuracy. By taking the time–frequency (TF) feature into account, TF-ESPRIT [10] shows its advantage in handling DOA estimation of wide-frequency nonstationary signals.

Considering the conflict between the number of detectable sources and the number of array sensors, many researchers have made great efforts, especially in the field of noncircular signal structures [11,12]. In addition to the normal covariance matrix, noncircular signals can provide extra information through the unconjugated spatial covariance matrix [13], thus the estimation accuracy is enhanced and the number of detectable sources is increased via joint analysis of both types of covariance matrices. This trick is accepted to modify subspace based DOA methods widely and a series of MUSIC-like [14–21] and ESPRIT-like [22–26] methods have been proposed. In the line of ESPRIT, the idea of joint analysis of both covariance matrices is first used in [22] and the method named NC-ESPRIT is proposed by Zoubir et al. Incorporating the forward–backward averaging and spatial smoothing, NC-Unitary-ESPRIT is addressed in [23] and can further lower the calculation complexity. For short snapshots, higher-order statistics are used and RNC-ESPRIT is presented in [24] to improve the estimation accuracy. To handle DOA estimation in shift-invariant R-D antenna arrays, R-D NC-Unitary-ESPRIT is proposed in [25].

Although these ESPRIT-like methods consider noncircular structures and break the conflict between the source number and sensor number in some sense, there are still some limitations,

* Corresponding author.
E-mail address: qiutsh@dlut.edu.cn (T. Qiu).

https://doi.org/10.1016/j.dsp.2019.01.018
1051-2004/

especially considering scenarios with impulsive noise [27,28]. In these situations, the noise often shows sudden bursts or sharp spikes [29,30], which in fact exhibits its non-Gaussian feature, and therefore the model of the impulsive noise is usually described by a type of non-Gaussian distribution, the alpha-stable distribution [31] or stable distribution for short. To solve the performance degradation of many methods based on second-order statistics including covariance under impulsive noise, many studies have been developed in many applications [32–37]. In this line, some novel concepts based on fractional lower-order statistics (FLOS) are proposed, such as covariation [32], fractional lower-order covariance (FLOC) [33] and phased fractional lower-order moment (PFLOM) [34], etc. Inspired by FLOS, a novel DOA estimation method termed NC-FLOS-ESPRIT was proposed recently in [35] to deal with the performance degeneration of NC-ESPRIT in scenarios of impulsive noise. It combines the idea of noncircular (NC) structures and the concept of FLOS to increase the estimation resolution and accuracy of the original ESPRIT for noncircular signals under impulsive noise.

Among the recent researches in stable distribution signal processing theory, a novel concept named bounded non-linear covariance (BNC) is proposed in [38] and it generalizes the concept of covariance and provides us a second choice when creating subspace matrices. Meanwhile, it conquers two main drawbacks of FLOS based methods, which are the dependence of the prior knowledge of noise and the suppression inefficiency of large outliers introduced by impulsive noise.

Considering these shortcomings of FLOS, a novel DOA estimation method based on subspace is proposed in this paper. It inherits the benefits from noncircular structure and BNC and is given the name NC-BNC-ESPRIT. Using BNC matrices, large outliers are suppressed more efficiently even with insufficient knowledge of impulsive noise. In addition, a more accurate DOA estimation is realized through the study of the rotational invariance of BNC matrices.

The remainder of this paper is organized as follows: In Section 2, the system model is described and the related works for NC-FLOS-ESPRIT are introduced as well as the works toward BNC. In Section 3, the procedure of BNC based ESPRIT for noncircular signals (NC-BNC-ESPRIT) is demonstrated. In Section 4, simulation results for the proposed method are provided and analysed. Finally, in Section 5, the conclusions are drawn. Other related mathematical proofs are provided in the Appendix.

Notation: In this paper, the bold letters denote matrices or column vectors; The superscripts $(\cdot)^*$, $(\cdot)^{\mathrm{T}}$, $(\cdot)^{\mathrm{H}}$ denote the complex conjugate, transpose and conjugate transpose, respectively; $\mathrm{E}[\cdot]$ stands for the statistical expectation; The operator $\mathrm{diag}\{\mathbf{a}\}$ returns a diagonal matrix with the elements of $\mathbf{a}$; The matrices $\mathbf{0}_M$ and $\mathbf{I}_M$ denote an $M \times M$ matrix of zeros and the identity matrix respectively.

2. Mathematical background

2.1. Alpha-stable distribution

To explain this problem clearly, we first introduce some concepts of the symmetric alpha-stable distribution for complex random variables. When there is a complex random variable that satisfies symmetric alpha-stable distribution, the characteristic function of the random variable is described as

$$\varphi(\omega) = \exp\left\{ j\mu\omega - \gamma|\omega|^{\alpha} \right\} \tag{1}$$

where α $(0 < \alpha \leq 2)$ is the characteristic exponent, γ $(\gamma > 0)$ represents the dispersion parameter which plays a similar role to that of the variance in the Gaussian distribution and μ $(-\infty < \mu < +\infty)$ is the location parameter. It has been proven that the Gaussian distribution derives from the alpha-stable distribution when $\alpha = 2$ [31].

When a received signal is interfered by symmetric alpha-stable distribution noise, it can be expressed as

$$x(t) = s(t) + v(t) \tag{2}$$

where $s(t)$ is the input signal, and $v(t)$ is the additive impulsive noise that subjects to alpha-stable distribution.

For DOA estimation, conventional ESPRIT methods use the second-order or higher-order statistics. For example, using second-order statistics, covariance is often used and calculated as

$$\begin{aligned} \mathrm{cov} &= \mathrm{E}\big[x(t)x(t)\big] \\ &= \mathrm{E}\big[s(t)s(t) + 2s(t)v(t) + v(t)v(t)\big] \end{aligned} \tag{3}$$

However, the moments whose orders are greater than α do not converge in the alpha-stable distribution. Therefore, when the noise is impulsive noise $(0 < \alpha < 2)$, $\mathrm{E}[v(t)v(t)] \to \infty$ and if $0 < \alpha < 1$, $\mathrm{E}[s(t)v(t)] \to \infty$. Such behaviour will lead to the covariance losing its efficiency for DOA estimation. Similar to covariance, other second-order or higher-order statistics are also proved to lose their abilities for DOA estimation under impulsive noise.

2.2. ULA model

Considering a uniform linear array (ULA) composed of M identical sensors with P independent far field narrow-band signals impinging on it. The distance between two adjacent sensors is d. Therefore, the signals received by the m-th sensor can be expressed as

$$x_m(t) = \sum_{i=1}^{P} s_i(t) \mathrm{e}^{-\mathrm{j}2\pi \sin(\theta_i)(m-1)d/\lambda} + n_m(t) \tag{4}$$

where θ_i represents the DOA of the i-th source signal $s_i(t)$, λ is the wavelength and $n_m(t)$ is the additive noise of the m-th sensor.

Collecting the M received signals in a vector form, the vector form of the received signals can be written as

$$\mathbf{x}(t) = \mathbf{A}(\theta)\mathbf{s}(t) + \mathbf{n}(t) \tag{5}$$

where $\mathbf{x}(t) = [x_1(t), x_2(t), \ldots, x_M(t)]^{\mathrm{T}}$ is the received signals vector, $\mathbf{s}(t) = [s_1(t), s_2(t), \ldots, s_P(t)]^{\mathrm{T}}$ is the source signals vector, $\mathbf{n}(t) = [n_1(t), n_2(t), \ldots, n_M(t)]^{\mathrm{T}}$ is the noises vector and $\mathbf{A}(\theta) = [\mathbf{a}(\theta_1), \mathbf{a}(\theta_2), \ldots, \mathbf{a}(\theta_P)]$ is the matrix for array steering where $\mathbf{a}(\theta_i) = [1, \mathrm{e}^{-\mathrm{j}2\pi \sin(\theta_i)d/\lambda}, \ldots, \mathrm{e}^{-\mathrm{j}2\pi \sin(\theta_i)(M-1)d/\lambda}]^{\mathrm{T}}$.

2.3. NC-FLOS-ESPRIT

Noncircular signals can be described as $\mathbf{s}(t) = \mathbf{\Phi}^{1/2}\mathbf{s}_0(t)$, where $\mathbf{s_0}(t) = [s_{01}(t), s_{02}(t), \ldots, s_{0P}(t)]^{\mathrm{T}}$ is the zero-phase version of signals and $\mathbf{\Phi}^{1/2} = \mathrm{diag}\{\mathrm{e}^{\mathrm{j}\phi_1/2}, \mathrm{e}^{\mathrm{j}\phi_2/2}, \ldots, \mathrm{e}^{\mathrm{j}\phi_P/2}\}$ is the noncircular phases of the signals [13]. Using the structure of the noncircular signals, described in [13], the extended array outputs $\mathbf{y}(t)$ noncircular signals is built as

$$\mathbf{y}(t) = \begin{bmatrix} \mathbf{x}(t) \\ \mathbf{x}^*(t) \end{bmatrix} \tag{6}$$

Conventional NC-ESPRIT methods exploit the covariance matrix of $\mathbf{y}(t)$ to estimate DOAs. Due to the performance degeneration of covariance based ESPRIT methods under impulsive noise, the NC-FLOS-ESPRIT algorithm was proposed by incorporating FLOS with NC-ESPRIT in [35] and covariation was used on the extended array to prove its efficiency.

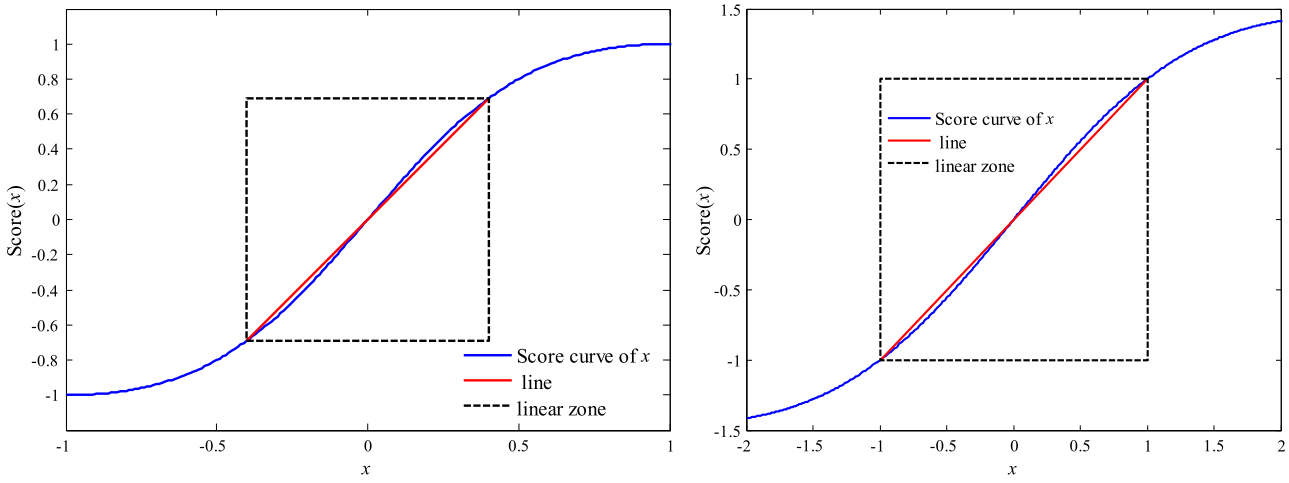

(a) score function with λ_3=λ_4=1 (b) score function with λ_3=0.4,λ_4=0.58

Fig. 1. Score BNC function with different parameters. (For interpretation of the colours in the figure(s), the reader is referred to the web version of this article.)

When two random variables satisfy a jointly symmetric alpha-stable distribution with characteristic exponent $1 < \alpha < 2$, the covariation of X and$Y$ is defined as

$$[X, Y]_\alpha = \frac{\mathrm{E}[XY^{\langle p-1\rangle}]}{\mathrm{E}[|Y|^p]}\gamma_Y, \quad 1 \le p < \alpha \tag{7}$$

where γ_Y represents the dispersion of Y and the operator $\langle\cdot\rangle$ represents the operation $Y^{\langle b\rangle} = |Y|^{b-1}Y^*$.

Applying the covariation on the extended array, a new covariation based matrix is proposed and it can be expressed as

$$\mathbf{G}_{nc} = \big[\mathbf{y}(t), \mathbf{y}(t)\big]_\alpha = \begin{bmatrix} \mathbf{A} \\ \mathbf{A}^*\boldsymbol{\Phi}^* \end{bmatrix} \boldsymbol{\Gamma}_{0\mathbf{s}} \begin{bmatrix} \mathbf{A} \\ \mathbf{A}^*\boldsymbol{\Phi}^* \end{bmatrix}^{\mathrm{H}} + \kappa_n \mathbf{I}_{2M} \tag{8}$$

where $\boldsymbol{\Gamma}_{0\mathbf{s}} = \mathrm{diag}\{\gamma_{01}, \gamma_{02}, \ldots, \gamma_{0P}\}$ is the diagonal covariation matrix of the signal vector $\mathbf{s}(t)$, in which $\gamma_{0k} = [s_{0k}(t), s_{0k}(t)]_\alpha$, and $\kappa_n = [n_i(t), n_j(t)]_\alpha$ is the covariation of noises. Similar to covariation, the fractional lower-order covariance (FLOC), the phased fractional lower-order moment (PFLOM) can also form the matrix $\mathbf{G}_{nc}$. Therefore, combining NC-ESPRIT with the FLOS based matrix $\mathbf{G}_{nc}$, DOA can be accurately estimated under impulsive noise.

Although these FLOS based matrices are efficient for suppressing the impulsive noise. There are still some limitations to these methods, such as the dependence of prior knowledge of noise and the significant degeneration of large outliers' suppression [39].

2.4. Bounded non-linear covariance

To realize efficient suppression of impulsive noise, especially for large outliers, Luan et al. proposed bounded non-linear covariance in [38] and the BNC function is defined as

$$g(x) = \begin{cases} f(x) & x \ge x_0 \\ l(x) & -x_0 < x < x_0 \\ f(x) & x \le -x_0 \end{cases} \tag{9}$$

where $l(x)$ and$f(x)$ are odd functions. Meanwhile, $l(x) \simeq x$ when $x \in (-x_0, x_0)$ and $f(x)$ satisfies $\max|f(x)| \le f_0$ for any given zero-mean variable. x_0 and f_0 are given constants and satisfy $f_0 > x_0 > 0$.

When considering array signal processing, the array signals are mostly complex. Therefore, the BNC matrix for the array output vector $\mathbf{x}$ is defined as

$$\mathbf{R}^{\mathrm{BNC}} = \mathrm{E}\big(g(\mathbf{x})g^{\mathrm{H}}(\mathbf{x})\big) \tag{10}$$

The score function is a typical BNC function that can be expressed as

$$\mathrm{score}(x) = \frac{2\lambda_4 \cdot x}{1 + (\lambda_3 \cdot x)^2} \tag{11}$$

where λ_3 and λ_4 are tunable parameters for adjusting the almost linear region of the signal.

To demonstrate the BNC function and tunable parameters more clearly, the score BNC function is shown in Fig. 1 with different tunable parameters.

Through Fig. 1(a), we find that the curve of the original score function appears to be almost linear within the range of $[-0.4, 0.4]$. To achieve an almost linear region within the range of $[-1, 1]$, we initialize the tunable parameters as $\lambda_3 = 0.4$ and $\lambda_4 = (1 + \lambda_3^2)/2 = 0.58$. The new curve is shown in Fig. 1(b). We observe that the original linear region is adjusted to the dashed line region where $x, y \in [-1, 1]$.

3. NC-BNC-ESPRIT

In DOA estimation, signals are usually assumed to be of zero mean value. Therefore, within a range around zero mean value, signals are weakly interfered with impulsive noise and have good information to realize DOA estimation. Meanwhile, from (9) and Fig. 1, we find that the BNC function is almost linear within the range around zero which means that it will retain the less interfered signals for DOA estimation. Otherwise, with extremely impulsive noise, the value of the signals is far from zero, and impulsiveness is suppressed efficiently by the BNC function which means that it has less effect on DOA estimation. Due to the properties in these two regions, the BNC function shows an efficient suppression of impulsive noise. Inspired by the efficient suppression of impulsive noise and the bounded property [38] of BNC, we propose a novel DOA estimation method named NC-BNC-ESPRIT. Combing the ideas of NC-ESPRIT with BNC, in the proposed method, the FLOS matrix from NC-FLOS-ESPRIT is replaced with a BNC matrix as follows

$$\mathbf{R}^{\mathrm{BNC}} = \mathrm{BNC}\big[\mathbf{y}(t), \mathbf{y}(t)\big] = \begin{bmatrix} \mathbf{R}^1_{\mathrm{BNC}} & \mathbf{R}^2_{\mathrm{BNC}} \\ \mathbf{R}^3_{\mathrm{BNC}} & \mathbf{R}^4_{\mathrm{BNC}} \end{bmatrix} \tag{12}$$

where the (i, j)th entries of these four sub-matrices $\mathbf{R}^1_{\mathrm{BNC}}, \mathbf{R}^2_{\mathrm{BNC}}, \mathbf{R}^3_{\mathrm{BNC}}, \mathbf{R}^4_{\mathrm{BNC}}$ are $\mathrm{BNC}(x_i(t), x_j(t))$, $\mathrm{BNC}(x_i(t), x_j^*(t))$, $\mathrm{BNC}(x_i^*(t), x_j(t))$

Table 1
The algorithm steps.

Algorithm steps	
1.	Calculate the $2M \times 2M$ BNC matrix $\mathbf{R}^{\mathrm{BNC}}$ and apply the eigenvalue decomposition to the BNC matrix as $\mathbf{R}^{\mathrm{BNC}} = \hat{\mathbf{U}}\hat{\Sigma}\hat{\mathbf{U}}^{\mathrm{H}}$
2.	Form the span signal subspace $\hat{\mathbf{U}}_{\mathbf{s}}$ with the largest P eigenvalues of $\mathbf{R}^{\mathrm{BNC}}$
3.	Use two selection matrices $\mathbf{J}_1$ and $\mathbf{J}_2$ to obtain the matrices $\hat{\mathbf{Q}}_1$ and $\hat{\mathbf{Q}}_2$ using $\hat{\mathbf{Q}}_2 = \mathbf{J}_2\hat{\mathbf{U}}_{\mathbf{s}}$, $\hat{\mathbf{Q}}_1 = \mathbf{J}_1\hat{\mathbf{U}}_{\mathbf{s}}$ where $\mathbf{J}_1 = \begin{bmatrix} \mathbf{T}_1 & \mathbf{0}_{(M-1)\times M} \\ \mathbf{0}_{(M-1)\times M} & \mathbf{T}_2 \end{bmatrix}$, $\mathbf{J}_2 = \begin{bmatrix} \mathbf{T}_2 & \mathbf{0}_{(M-1)\times M} \\ \mathbf{0}_{(M-1)\times M} & \mathbf{T}_1 \end{bmatrix}$ and $\mathbf{T}_1 = [\mathbf{I}_{(M-1)\times(M-1)}\mathbf{0}_{(M-1)\times 1}]$, $\mathbf{T}_2 = [\mathbf{0}_{(M-1)\times 1}\mathbf{I}_{(M-1)\times(M-1)}]$
4.	Compute the eigenvalues $e^{-j\psi_1}, e^{-j\psi_2}, \ldots, e^{-j\psi_P}$ of matrix $\hat{\mathbf{Q}} = (\hat{\mathbf{Q}}_1^{\mathrm{H}}\hat{\mathbf{Q}}_1)^{-1}\hat{\mathbf{Q}}_1^{\mathrm{H}}\hat{\mathbf{Q}}_2$
5.	Obtain the DOAs using $\theta_i = \arcsin(\frac{\lambda \arg(\psi_i)}{2\pi d})$ $i = 1, 2, \ldots, P$

and $\mathrm{BNC}(x_i^*(t), x_j^*(t))$. In addition, this BNC matrix can be expressed as

$$\mathbf{R}^{\mathrm{BNC}} = \begin{bmatrix} \mathbf{A} \\ \mathbf{A}^*\boldsymbol{\Phi}^* \end{bmatrix} \mathbf{R}_{0\mathbf{s}}^{\mathrm{BNC}} \begin{bmatrix} \mathbf{A} \\ \mathbf{A}^*\boldsymbol{\Phi}^* \end{bmatrix}^{\mathrm{H}} + \sigma_n^2 \mathbf{I}_{2M} \tag{13}$$

where $\mathbf{R}_{0\mathbf{s}}^{\mathrm{BNC}} = \mathrm{diag}\{\nu_{01}, \nu_{02}, \ldots, \nu_{0P}\}$ is the diagonal BNC matrix for the signal $\mathbf{s}(t)$, in which $\nu_{0k} = \mathrm{BNC}(s_{0k}(t), s_{0k}(t))$ and σ_n is the variance of the approximate noise. The detailed proof for (13) is presented in Appendix A.

Then, the steering matrix $\mathbf{B}$ can be obtained as

$$\mathbf{B} = \begin{bmatrix} \mathbf{A} \\ \mathbf{A}^*\boldsymbol{\Phi}^* \end{bmatrix} = \left[\mathbf{b}(\theta_1, \phi_1), \mathbf{b}(\theta_2, \phi_2), \ldots, \mathbf{b}(\theta_P, \phi_P)\right] \tag{14}$$

where $\mathbf{b}(\theta_i, \phi_i)$ contains the DOAs information of signals and it can be expressed as

$$\mathbf{b}(\theta_i, \phi_i) = \left[1, e^{-j\psi_i}, \ldots, e^{-j(M-1)\psi_i}, e^{-j\phi_i}, e^{j\psi_i}e^{-j\phi_i}, \ldots, e^{j(M-1)\psi_i}e^{-j\phi_i}\right]^{\mathrm{T}} \tag{15}$$

with $\psi_i = 2\pi \sin(\theta_i)d/\lambda$.

Obviously, the structure of the proposed BNC matrix is similar in form with the covariation based matrix in (8). Therefore, similar to NC-FLOS-ESPRIT, the DOAs are obtained by the follow steps in Table 1.

4. Simulations

4.1. Computational complexity analysis

In this section, we analyse the computational complexity via time complexity. In the process of NC-BNC-ESPRIT, the computation differs from that of other methods only in the covariance calculation. In this paper, we use the score function as the BNC function. From (10) and (11), we find that the time complexity of the BNC calculation is $O(n^4)$, where n is the limited snapshots of signals. Although this complexity is more than that of conventional NC-ESPRIT: $O(n^2)$ or NC-FLOS-ESPRIT: $O(n^p)$, $p < 2$, it is still not sufficiently large to influence the real-time performance of computation.

4.2. Comprehensive simulations

In this section, a series of simulations are implemented to evaluate the performance of the proposed method. Two typical noncircular signals (BPSK) are used as input signals. It is assumed that these two input signals imping on a ULA with 5 sensors. The DOAs of these two signals are set to $\theta_1 = 5°$ and $\theta_2 = 15°$. The interference noises satisfy a complex symmetric alpha-stable distribution. Because the variance of the noise is not convergent under alpha-stable distribution, the generalized signal ratio to noise (GSNR) is defined as

$$\mathrm{GSNR} = 10\lg(Pw/\gamma) \tag{16}$$

where Pw is the signal power and γ is the noise dispersion.

The proposed method is compared with six existing methods, namely, NC-ESPRIT [22], NC-MUSIC [17], l_p-ESPRIT [41], NC-Unitary-ESPRIT [23], NC-FLOS-ESPRIT [35] and our recent work against impulsive noise by maximum correntropy criterion based MUSIC (MCC-MUSIC) [42]. According to [35,40], the parameter p of these FLOS based methods is set to 1. In the simulations, score function is chosen as the BNC function and the tunable parameters are set to $\lambda_3 = 0.4$ and $\lambda_4 = (1 + \lambda_3^2)/2 = 0.58$ according to [38]. The following experiments are performed with the change of four parameters, the characteristic exponent α, the GSNR defined by (16), the length of snapshots and the source angular separation. Because performances with different α or GSNRs can demonstrate the resistant abilities of different methods to impulsive noise, and performances with different snapshots or source angular separations can reflect the resolution abilities of different methods. To elaborate the performances, two quantities named probability of resolution and root mean square error (RMSE) are measured for 200 Monte-Carlo experiments.

In the experiments, a successful resolution of DOA is defined as

$$\left(\hat{\theta}_i(k) - \theta_i\right) \le 1° \quad \text{for both } i = 1 \text{ and } i = 2 \tag{17}$$

where θ_i and $\hat{\theta}_i(k)$ represent the true value of the i-th DOA and the estimated value of the k-th DOA in the total Monte-Carlo experiments. Therefore, the probability of resolution is defined as the ratio of the number of successful resolutions to the total number of experiments runs.

Then the RMSE can be calculated as

$$\mathrm{RMSE} = \sqrt{\frac{1}{L_S P}\sum_{k=1}^{L_S}\sum_{i=1}^{P}\left(\hat{\theta}_i(k) - \theta_i\right)^2} \tag{18}$$

where L_S is the number of successful estimations in the Monte-Carlo experiments.

4.2.1. Simulation with more sources than sensors

Using the properties of noncircular signals, the proposed method will still be efficient when the number of sources is more than sensors. To demonstrate the efficiency of the algorithm, a simulation is performed in this part with more sources than sensors. The number of sensors in the ULA is set to 3, and the number of sources is set to 4 with different DOAs of $[-20°, 0°, 10°, 30°]$. The characteristic exponent of impulsive noise is set to $\alpha = 1.6$, the snapshot is set to 300 and we focus on the performance of the proposed method when GSNR ranges from 10 dB to 20 dB. The simulation result is shown in Fig. 2.

From the simulation results shown in Fig. 2, we find that the conventional ESPRIT method lose its efficiency on DOA estimation when the number of sources is larger than the number of sensors. However, the accuracy of the proposed method is more than 50% when GSNR exceeds 11 dB, which indicates the efficiency of the proposed method for solving the conflict between the source number and the sensor number.

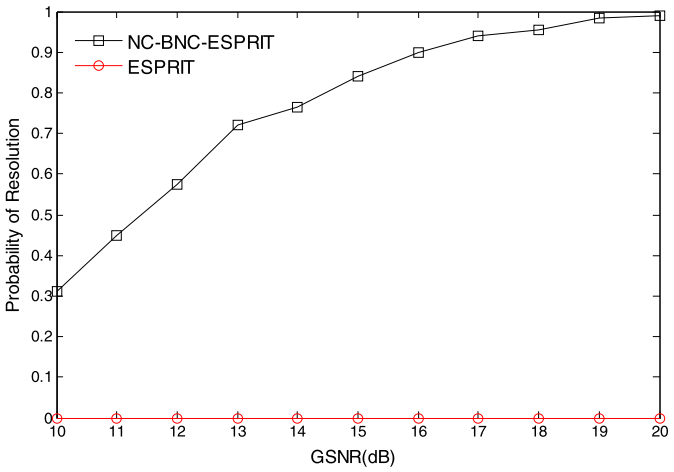

Fig. 2. Resolution probability for different GSNRs with more sources than sensors.

4.2.2. Experiment with different characteristic exponents

In this experiment, the effects of different characteristic exponents of noise on DOAs estimation are measured. The characteristic exponent α of impulsive noise ranges from 1.1 to 2. The GSNR condition remains unchanged at 10 dB. The length of signals' snapshots received for each sensor is set to 300. The performances of different methods are evaluated in Fig. 3.

From the results of the simulations, we observe that the resolution probabilities of all methods increase and their RMSEs show a downward trend when the characteristic exponent changes from 1.1 to 2, which corresponds to a transition from impulsive noise to Gaussian noise. Compared with other methods, our method shows equivalent performance with less impulsive noise ($\alpha > 1.7$) which the noise is close to Gaussian noise. This result indicates that our method is robust not only for impulsive noise but also for Gaussian noise. Considering the highly impulsive situations ($\alpha < 1.5$), only our method, NC-FLOS-ESPRIT, MCC-MUSIC and l_p-ESPRIT show good performances due to their resistance to impulsive noise and the second-order statistics based methods lose their efficiency in such extremely impulsive noise. Among these efficient methods, our method achieves a best performance than others due to its superior suppression of large outliers and application of the signals' noncircular structure.

4.2.3. Experiment with different GSNRs

In this experiment, the effects of different GSNR conditions on DOAs estimation are evaluated. We consider that signals are interfered by a fair impulsive noise condition, when the GSNR ranges from 6 dB to 15 dB, the characteristic exponent is set as $\alpha = 1.6$. The number of signals' snapshots is set to 300. The performances of different methods are shown in Fig. 4.

According to the simulation results in Fig. 4, we find that the performances of all methods are improved in terms of resolution probability and RMSE as expected, because the noise interference decreases with increasing GSNR. For moderate impulsive noise environments (GSNR $>$ 10 dB), most methods show good performances. Among them, our method, NC-FLOS-ESPRIT, MCC-MUSIC and l_p-ESPRIT demonstrate better performances due to their resistance to impulsive noise. However, for low GSNR conditions (GSNR $<$ 9 dB) where the impulsive noise becomes strong, conventional methods exhibit performance degeneration. Among these efficient methods, our method and NC-FLOS-ESPRIT show higher resolution probabilities and lower RMSEs than others because they also exploit the noncircular structures of signals. Furthermore, our method presents a better performance than NC-FLOS-ESPRIT in terms of resolution probability as well as RMSE under highly impulsive noise environments because of its superior suppression of large outliers.

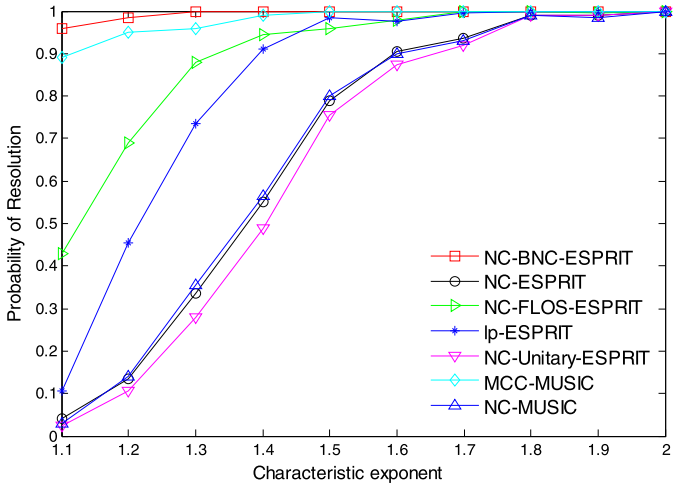

(a) Probability of resolution for different characteristic exponents α

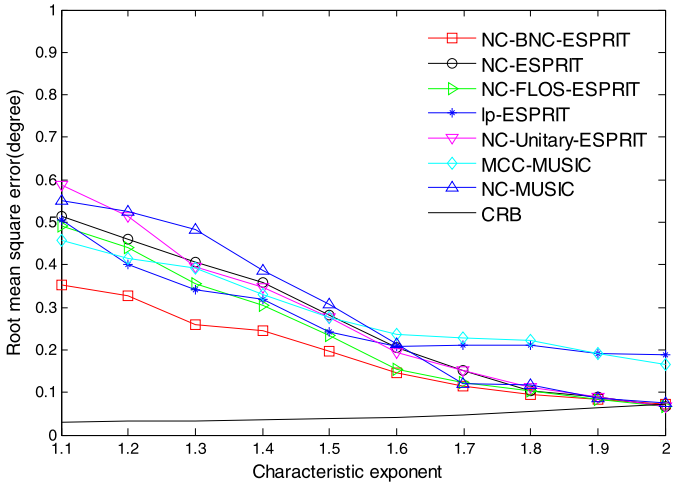

(b) RMSE for different characteristic exponents α

Fig. 3. Experimental results with different characteristic exponents α.

4.2.4. Experiment with different snapshots

In this experiment, the effects of different snapshots of signals on DOAs estimation are presented. As we increase the number of snapshots of signals from 50 to 800, a gentle impulsive noise environment is considered with $\alpha = 1.6$ and GSNR is set to 10 dB. The performances of different methods are illustrated in Fig. 5.

Through the simulation results shown in Fig. 5, we find that when the snapshots become longer, only our method, NC-FLOS-ESPRIT, MCC-MUSIC and l_p-ESPRIT still maintain good performances. By contrast, other second-order statistics based methods display a performance deterioration with the increase of snapshot due to the impulsive noise interference becoming stronger when more noise samples are integrated to data and these methods do not have the resistance to impulsive noise. Among these efficient methods, our method shows the best performance than others both in terms of resolution probability and RMSE owing to the application of noncircular structure of the signals and its superior suppression of large outliers.

4.2.5. Experiment with different source angular separations

In this experiment, the effects of different angular separations on DOAs estimation are introduced. The angle of the two signals are separated from 4° to 15° under a moderate situation in which

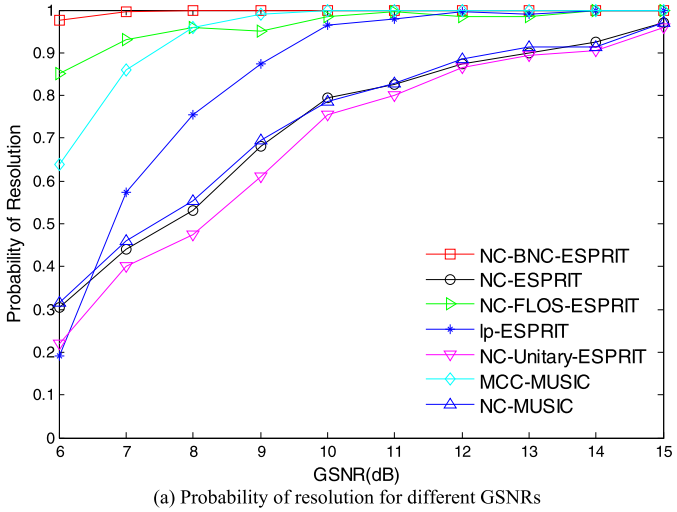

(a) Probability of resolution for different GSNRs

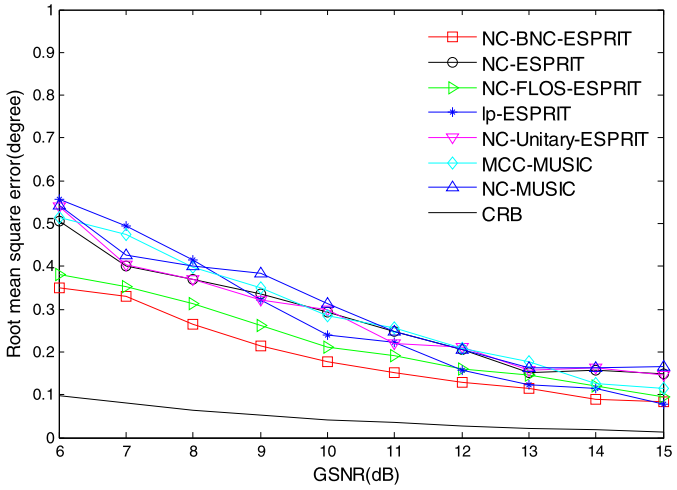

(b) RMSE for different GSNRs

Fig. 4. Experimental results with different GSNRs.

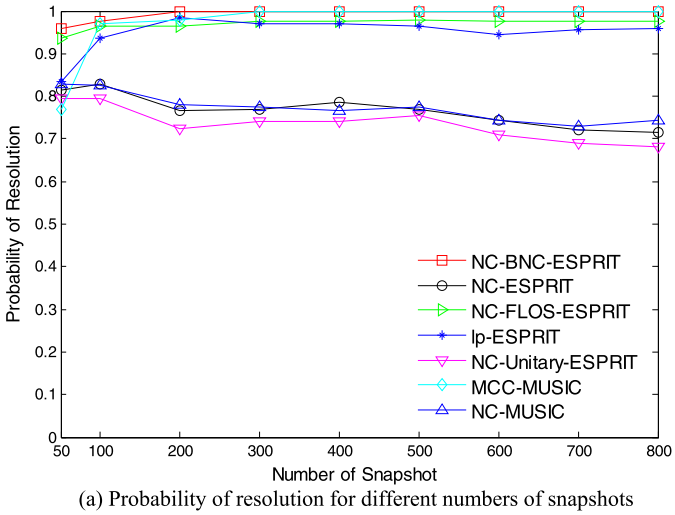

(a) Probability of resolution for different numbers of snapshots

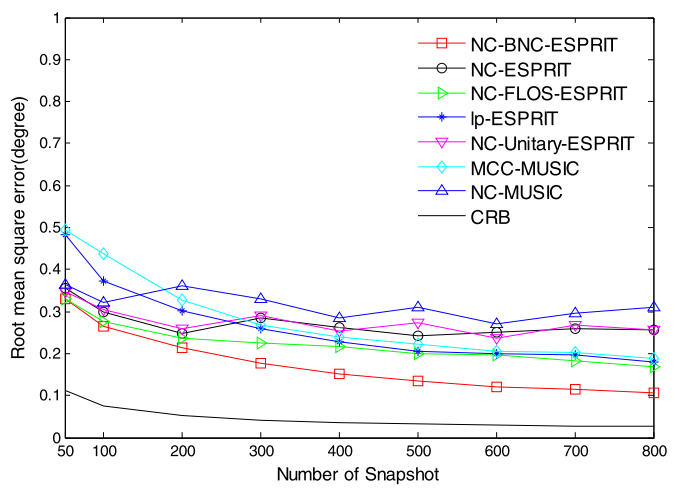

(b) RMSE for different snapshots

Fig. 5. Experimental results for different numbers of snapshots.

$\alpha = 1.6$ and GSNR is set to 10 dB. The number of snapshots is set to 300. The performances of the different methods are demonstrated in Fig. 6.

From the simulation results illustrated in Fig. 6, we observe that all methods show better performances with larger angular separations. This is because the signals are more easily distinguishable and less cluttered with each other when the angular separation is larger. For situations with large angular separation ($\geq 7°$), our method, NC-FLOS-ESPRIT, MCC-MUSIC and l_p-ESPRIT achieve better performances than the other NC based methods because of the resistance to impulsive noise and the deterioration of second-order statistics based methods under such noise. Furthermore, for conditions with less angular separation ($< 7°$), our method and NC-FLOS-ESPRIT perform better than others with the help of a noncircular structure. Otherwise, our method presents a better performance than NC-FLOS-ESPRIT in all situations due to its efficient suppression of large outliers, and it can achieve a completely successful resolution of the signals when the angular separation is more than 4°.

5. Conclusions

In this paper, we propose an accurate and robust DOA estimation method for noncircular signals. To improve the performance for DOA estimation interfered by impulsive noise, we propose a NC-BNC-ESPRIT by constructing a BNC matrix of extended array output. By exploiting the rotational invariance of the BNC matrix, the estimation performance of DOA is improved significantly. To evaluate the proposed method, it is compared with six other methods via the probability of resolution and RMSE. Simulation results verify that the proposed method has a significant advantage over other methods under impulsive noise environment, particularly in low GSNRs and extremely impulsive situations. However, the proposed method is only applicable for uniform linear arrays. Considering many other practical applications, further works are needed to solve DOA estimation for other conditions under impulsive noise, such as uniform circular arrays (UCA), multiple-input multiple-output (MIMO) radar systems and so on.

Conflict of interest statement

There is no conflict of interest.

Acknowledgments

This study is supported partly by the National Natural Science Foundation of China (61172108, 61139001, 81241059, 61501301, 61801197), the Jiangsu Natural Science Foundation (Grant No. BK20181004) and the National Science Foundation of the Jiangsu Higher Education Institutions of China (Grant No. 18KJB510012).

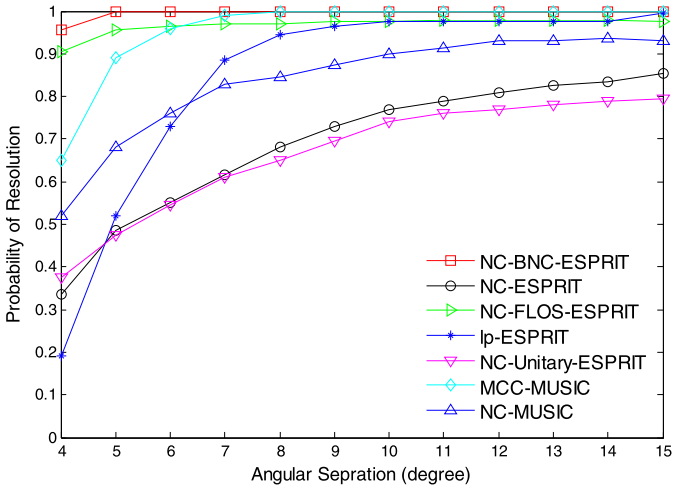

(a) Probability of resolution for different angular separations

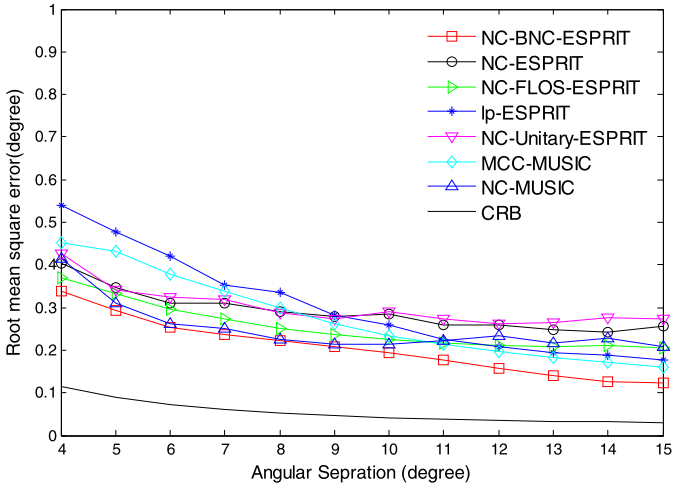

(b) RMSE for different angular separations

Fig. 6. Experimental results for different angular separations.

Appendix A. A brief interpretation of the proof for (13)

To calculate the four sub-matrices in (13), we analyse the first sub-matrix $\mathbf{R}^1_{\mathrm{BNC}}$. To extract the DOAs from the received signals, the information of sample points with less impulsive noise interference should be used. From the expression of the BNC function in (9), we find that the BNC function is almost linear for the samples with less noise interference.

Therefore, supposing $x_i(t)$ and $x_j(t)$ locate in the almost linear region of the BNC function, the (i, j)th entries of $\mathbf{R}^1_{\mathrm{BNC}}$ can be written as

$$\begin{aligned} r^1_{ij} &= \mathrm{BNC}\big(x_i(t), x_j(t)\big) \\ &= \mathrm{BNC}\big(\mathbf{A}_i(\theta)\mathbf{s}(t) + n_i(t), \mathbf{A}_j(\theta)\mathbf{s}(t) + n_j(t)\big) \\ &= \mathrm{E}\big[g\big(\mathbf{A}_i(\theta)\mathbf{s}(t) + n_i(t)\big)g^{\mathrm{H}}\big(\mathbf{A}_j(\theta)\mathbf{s}(t) + n_j(t)\big)\big] \end{aligned} \tag{19}$$

where $\mathbf{A}_i(\theta) = [\mathrm{e}^{-\mathrm{j}2\pi\sin(\theta_1)d(i-1)/\lambda}, \ldots, \mathrm{e}^{-\mathrm{j}2\pi\sin(\theta_P)d(i-1)/\lambda}]$. When $x_i(t)$ and $x_j(t)$ locate in the almost linear region, we can approximate the impulse noise as the Gaussian noise because of the suppression of impulsive noise by BNC. Due to the independence between signals and noise, we can represent r^1_{ij} as

$$\begin{aligned} r^1_{ij} &= \mathrm{E}\big[\big(\big(g\big(\mathbf{A}_i(\theta)\mathbf{s}(t)\big) + n^{\mathrm{G}}_i(t)\big)\big)\big(\big(g^{\mathrm{H}}\big(\mathbf{A}_j(\theta)\mathbf{s}(t)\big) + \big(n^{\mathrm{G}}_j(t)\big)^{\mathrm{H}}\big)\big)\big] \\ &= \mathrm{BNC}\big(\mathbf{A}_i(\theta)\mathbf{s}(t), \mathbf{A}_j(\theta)\mathbf{s}(t)\big) + \mathrm{E}\big(n^{\mathrm{G}}_i(t), \big(n^{\mathrm{G}}_j(t)\big)^{\mathrm{H}}\big) \end{aligned} \tag{20}$$

where $n^{\mathrm{G}}_i(t)$ and $n^{\mathrm{G}}_j(t)$ represent the approximation of $n_i(t)$ and $n_j(t)$ with variance σ_n. From [13], we know that the noncircular signal can be described as $\mathbf{s}(t) = \mathbf{\Phi}^{1/2}\mathbf{s}_0(t)$ where $\mathbf{s_0}(t) = [s_{01}(t), s_{02}(t), \ldots, s_{0P}(t)]^{\mathrm{T}}$ is the zero-phase version of signals and $\mathbf{\Phi}^{1/2} = \mathrm{diag}\{\mathrm{e}^{\mathrm{j}\phi_1/2}, \mathrm{e}^{\mathrm{j}\phi_2/2}, \ldots, \mathrm{e}^{\mathrm{j}\phi_P/2}\}$ are the noncircular phases of the signals.

Therefore, the first item of r^1_{ij} can be described as

$$\begin{aligned} &\mathrm{BNC}\big(\mathbf{A}_i(\theta)\mathbf{s}(t), \mathbf{A}_j(\theta)\mathbf{s}(t)\big) \\ &= \mathrm{BNC}\left(\sum_{k=1}^{P} a_k(\theta)\mathrm{e}^{\mathrm{j}\phi_k/2}s_{0k}(t), \sum_{u=1}^{P} a_u(\theta)\mathrm{e}^{\mathrm{j}\phi_u/2}s_{0u}(t)\right) \end{aligned} \tag{21}$$

According to the independent property of BNC (for the detailed proof refer to [38]), formula (21) is given as

$$\begin{aligned} &\mathrm{BNC}\big(\mathbf{A}_i(\theta)\mathbf{s}(t), \mathbf{A}_j(\theta)\mathbf{s}(t)\big) \\ &= \sum_{k=1}^{P} a_i(\theta_k)\mathrm{e}^{\mathrm{j}\phi_k/2}\big(\big(a_j(\theta_k)\mathrm{e}^{\mathrm{j}\phi_k/2}\big)^*\big)\mathrm{BNC}\big(s_{0k}(t), s_{0k}(t)\big) \\ &= \sum_{k=1}^{P} a_i(\theta_k)a^*_j(\theta_k)\nu_{0k} \end{aligned} \tag{22}$$

where $\nu_{0k} = \mathrm{BNC}(s_{0k}(t), s_{0k}(t))$.

In addition, the noise part $\mathrm{E}(n^{\mathrm{G}}_i(t)(n^{\mathrm{G}}_j(t))^{\mathrm{H}})$ can be written as $\mathrm{E}(n^{\mathrm{G}}_i(t)(n^{\mathrm{G}}_j(t))^{\mathrm{H}}) = \sigma^2_n\delta_{i,j}$.

Therefore, the final expression for $\mathbf{R}^1_{\mathrm{BNC}}$ is

$$\mathbf{R}^1_{\mathrm{BNC}} = \sum_{k=1}^{P} a_i(\theta_k)a^*_j(\theta_k)\nu_{0k} + \sigma^2_n\delta_{i,j} \tag{23}$$

Through similar analysis of $\mathbf{R}^1_{\mathrm{BNC}}$, the other three sub-matrices are obtained as

$$\mathbf{R}^2_{\mathrm{BNC}} = \sum_{k=1}^{P} a_i(\theta_k)a_j(\theta_k)e^{\mathrm{j}\phi k}\nu_{0k} \tag{24}$$

$$\mathbf{R}^3_{\mathrm{BNC}} = \sum_{k=1}^{P} a^*_i(\theta_k)a^*_j(\theta_k)e^{-\mathrm{j}\phi k}\nu_{0k} \tag{25}$$

$$\mathbf{R}^4_{\mathrm{BNC}} = \sum_{k=1}^{P} a^*_i(\theta_k)a_j(\theta_k)\nu_{0k} + \sigma^2_n\delta_{i,j} \tag{26}$$

Integrating these four sub-matrices, the extended BNC matrix can be written as

$$\mathbf{R}^{\mathrm{BNC}} = \begin{bmatrix} \mathbf{A} \\ \mathbf{A}^*\mathbf{\Phi}^* \end{bmatrix}\mathbf{R}^{\mathrm{BNC}}_{\mathbf{0s}}\begin{bmatrix} \mathbf{A} \\ \mathbf{A}^*\mathbf{\Phi}^* \end{bmatrix}^{\mathrm{H}} + \sigma^2_n\mathbf{I}_{2M} \tag{27}$$

End of Proof.

References

[1] H. Krim, M. Viberg, Two decades of array signal processing research: the parametric approach, IEEE Signal Process. Mag. 13 (4) (1996) 67–94.
[2] R. Schmidt, Multiple emitter location and signal parameter estimation, IEEE Trans. Antennas Propag. 34 (3) (1986) 276–280.
[3] B.D. Rao, K.V.S. Hari, Performance analysis of root-MUSIC, IEEE Trans. Acoust. Speech Signal Process. 37 (12) (1989) 1939–1949.
[4] C. Qian, L. Huang, Y. Xiao, H.C. So, Two-step reliability test based unitary root-MUSIC for direction-of-arrival estimation, Digit. Signal Process. 44 (2015) 68–75.
[5] F.K. Gruber, E.A. Marengo, A.J. Devaney, Time-reversal imaging with multiple signal classification considering multiple scattering between the targets, J. Acoust. Soc. Am. 115 (6) (2004) 3042–3047.

[6] D. Ciuonzo, G. Romano, R. Solimene, Performance analysis of time-reversal MUSIC, IEEE Trans. Signal Process. 63 (10) (2015) 2650–2662.
[7] D. Ciuonzo, P.S. Rossi, Noncolocated time-reversal MUSIC: high-SNR distribution of null spectrum, IEEE Signal Process. Lett. 24 (4) (2017) 397–401.
[8] R. Roy, T. Kailath, ESPRIT-estimation of signal parameters via rotational invariance techniques, IEEE Trans. Acoust. Speech Signal Process. 37 (7) (1989) 984–995.
[9] A.N. Lemma, A.J. Van der Veen, E.F. Deprettere, Multiresolution ESPRIT algorithm, IEEE Trans. Signal Process. 47 (6) (1999) 1722–1726.
[10] J.C. Lin, X.C. Ma, S.F. Yan, et al., Time-frequency multi-invariance ESPRIT for DOA estimation, IEEE Antennas Wirel. Propag. Lett. 15 (2016) 770–773.
[11] D.P. Mandic, V.S.L. Goh, Complex Valued Nonlinear Adaptive Filters: Noncircularity, Widely Linear and Neural Models, John Wiley & Sons, 2009.
[12] B. Picinbono, P. Chevalier, Widely linear estimation with complex data, IEEE Trans. Signal Process. 43 (1995) 2030–2033.
[13] J.P. Delmas, Asymptotically minimum variance second-order estimation for noncircular signals with application to DOA estimation, IEEE Trans. Signal Process. 52 (5) (2004) 1235–1241.
[14] P. Gounon, C. Adnet, J. Galy, Localization angulaire de signaux non circulaires, Trait. Signal 15 (1) (1998) 17–23.
[15] P. Chargé, Y. Wang, J. Saillard, A non-circular sources direction finding method using polynomial rooting, Signal Process. 81 (8) (2001) 1765–1770.
[16] J. Liu, Z.T. Huang, Y.Y. Zhou, Extended 2q-MUSIC algorithm for noncircular signals, Signal Process. 88 (6) (2008) 1327–1339.
[17] H. Abeida, J.P. Delmas, MUSIC-like estimation of direction of arrival for noncircular sources, IEEE Trans. Signal Process. 54 (7) (2006) 2678–2690.
[18] F. Gao, A. Nallanathan, Y. Wang, Improved MUSIC under the coexistence of both circular and noncircular sources, IEEE Trans. Signal Process. 56 (7) (2008) 3033–3038.
[19] J.F. Li, D. Li, D.F. Jiang, et al., Extended-aperture unitary root MUSIC based DOA estimation for coprime array, IEEE Commun. Lett. 14 (8) (2018) 752–755.
[20] H. Zhai, X.F. Zhang, W. Zheng, DOA estimation of noncircular signals for coprime linear array via locally reduced-dimensional capon, Int. J. Electron. 105 (5) (2018) 709–724.
[21] F.G. Sun, Q.H. Wu, Y.M. Sun, et al., An iterative approach for sparse direction-of-arrival estimation in co-prime arrays with off-grid targets, Digit. Signal Process. 61 (2017) 35–42.
[22] A. Zoubir, P. Chargé, Y. Wang, Non circular sources localization with ESPRIT, in: Proceedings of European Conference on Wireless Technology, ECWT 2003, Munich, Germany, 2003.
[23] M. Haardt, F. Romer, Enhancements of unitary ESPRIT for non-circular sources, in: Proceedings of IEEE International Conference on Acoustics, Speech, and Signal Processing, ICASSP'04, Montreal, Canada, 2004, pp. 101–104.
[24] W.J. Si, Q.Q. Lin, Robust direction finding algorithm for non-circular signals, J. Syst. Eng. Electron. 35 (3) (2013) 469–473.
[25] J. Steinwandt, F. Roemer, M. Haardt, et al., R-dimensional ESPRIT-type algorithms for strictly second-order non-circular sources and their performance analysis, IEEE Trans. Signal Process. 62 (18) (2014) 4824–4838.
[26] J. Steinwandt, F. Roemer, M. Haardt, et al., Performance analysis of multi-dimensional ESPRIT-type algorithms for arbitrary and strictly non-circular sources with spatial smoothing, IEEE Trans. Signal Process. 65 (9) (2017) 2262–2276.
[27] A. Ahandra, Measurements of radio impulsive noise from various sources in an indoor environment at 900 MHz and 1800 MHz, in: Proceedings of the 13th IEEE International Symposium on Personal, Indoor and Mobile Radio Communications, vol. 2, 2002, pp. 639–643.
[28] J. He, Z. Liu, Underwater acoustic azimuth and elevation angle estimation using spatial invariance of two identically oriented vector hydrophones at unknown locations in impulsive noise, Digit. Signal Process. 19 (3) (2009) 452–462.
[29] M.D. Button, J.G. Gardiner, I.A. Glover, Measurement of the impulsive noise environment for satellite-mobile radio systems at 1.5 GHz, IEEE Trans. Veh. Technol. 51 (3) (2002) 551–560.
[30] K.L. Blackard, T.S. Rappaport, C.W. Bostian, Measurements and models of radio frequency impulsive noise for indoor wireless communications, IEEE J. Sel. Areas Commun. 11 (7) (1993) 991–1001.
[31] C.L. Nikias, M. Shao, Signal Processing with Alpha-Stable Distributions and Applications, Wiley–Interscience, 1995.
[32] P. Tsakalides, C.L. Nikias, The robust covariation-based MUSIC (ROC-MUSIC) algorithm for bearing estimation in impulsive noise environments, IEEE Trans. Signal Process. 44 (7) (1996) 1623–1633.
[33] D.F. Zha, T.S. Qiu, Underwater sources location in non-Gaussian impulsive noise environments, Digit. Signal Process. 16 (2) (2006) 149–163.
[34] H. Belkacemi, S. Marcos, Robust subspace-based algorithms for joint angle/Doppler estimation in non-Gaussian clutter, Signal Process. 87 (7) (2007) 1547–1558.
[35] J.F. Zhang, T.S. Qiu, The fractional lower order moments based ESPRIT algorithm for noncircular signals in impulsive noise environments, Wirel. Pers. Commun. 96 (2) (2017) 1673–1690.
[36] S.P. Talebi, S. Werner, D.P. Mandic, Distributed adaptive filtering of stable signals, IEEE Signal Process. Lett. 25 (10) (2018) 1450–1454.
[37] S.P. Talebi, D.P. Mandic, Distributed particle filtering of stable signals, IEEE Signal Process. Lett. 24 (12) (2017) 1862–1866.
[38] S.Y. Luan, T.S. Qiu, L. Yu, et al., BNC-based projection approximation subspace tracking under impulsive noise, IET Radar Sonar Navig. 11 (7) (2017) 1055–1061.
[39] L. Yu, T.S. Qiu, S.Y. Luan, Robust joint estimation for time delay and Doppler frequency shift based on generalised sigmoid cyclic cross-ambiguity function, IET Radar Sonar Navig. 11 (5) (2016) 721–728.
[40] J.F. Zhang, T.S. Qiu, A novel covariation based noncircular sources direction finding method under impulsive noise environments, Signal Process. 98 (2014) 252–262.
[41] W.J. Zeng, H.C. So, L. Huang, l_p-MUSIC: robust direction-of-arrival estimator for impulsive noise environments, IEEE Trans. Signal Process. 61 (17) (2013) 4296–4308.
[42] P. Wang, T.S. Qiu, F.Q. Ren, et al., A robust DOA estimator based on the correntropy in alpha-stable noise environments, Digit. Signal Process. 60 (2017) 242–251.

Jiacheng Zhang is now pursing the Ph.D. degree in signal and information processing at Dalian University of Technology, Dalian Liaoning, China. He received the B.S. degree and M.S. degree from the School of Biomedical Engineering, Dalian University of Technology in 2015 and 2018, respectively. His research interests are mainly focused on non-Gaussian signal processing and parameter estimation.

Tianshuang Qiu is a professor in the Faculty of Electronic Information and Electrical Engineering, Dalian University of Technology, Dalian Liaoning, China. He received the B.S. degree from Tianjin University, Tianjin, China, in 1983, and the M.S. degree from Dalian University of Technology, Dalian, China, in 1993, and the Ph.D. degree from Southeastern University, Nanjing, China, in 1996, all in electrical engineering. He worked as a postdoctoral fellow in the Department of Electrical Engineering at Northern Illinois University, USA, from 1996 to 2000. His research interests include wireless signal processing, biomedical signal processing, and non-Gaussian signal processing.

Shengyang Luan is a lecturer in the School of Electrical Engineering and Automation, Jiangsu Normal University, Xuzhou Jiangsu, China. His research interests include non-Gaussian signal processing and array signal processing.

Houjie Li is a lecturer in the College of Information and Communication Engineering, Dalian Minzu University, Dalian Liaoning, China. His research interests include image processing and Deep Learning.